The Cerebellum (2019) 18:22–32
https://doi.org/10.1007/s12311-018-0936-3

ORIGINAL PAPER

Far-infrared Radiation Improves Motor Dysfunction and Neuropathology in Spinocerebellar Ataxia Type 3 Mice

Shin-Wu Liu[1] · Jui-Chih Chang[1] · Sheng-Fei Chuang[1] · Ko-Hung Liu[1] · Wen-Ling Cheng[1] · Hui-Ju Chang[1] · Huei-Shin Chang[1] · Ta-Tsung Lin[1] · Ching-Liang Hsieh[2,3] · Wei-Yong Lin[3,4] · Mingli Hsieh[5] · Shou-Jen Kuo[6] · Chin-San Liu[1,3,7]

Published online: 3 May 2018

Abstract

Spinocerebellar ataxia type 3 (SCA3) is a polyglutamine neurodegenerative disease resulting from the misfolding and accumulation of a pathogenic protein, causing cerebellar dysfunction, and this disease currently has no effective treatments. Far-infrared radiation (FIR) has been found to protect the viability of SCA3 cells by preventing mutant ataxin-3 protein aggregation and promoting autophagy. However, this possible treatment still lacks in vivo evidence. This study assessed the effect of FIR therapy on SCA3 in vivo by using a mouse model over 28 weeks. Control mice carried a healthy wild-type ATXN3 allele that had a polyglutamine tract with 15 CAG repeats (15Q), whereas SCA3 transgenic mice possessed an allele with a pathological polyglutamine tract with expanded 84 CAG (84Q) repeats. The results showed that the 84Q SCA3 mice displayed impaired motor coordination, balance abilities, and gait performance, along with the associated loss of Purkinje cells in the cerebellum, compared with the normal 15Q controls; nevertheless, FIR treatment was sufficient to prevent those defects. FIR significantly improved performance in terms of maximal contact area, stride length, and base support in the forepaws, hindpaws, or both. Moreover, FIR treatment supported the survival of Purkinje cells in the cerebellum and promoted the autophagy, as reflected by the induction of autophagic markers, LC3II and Beclin-1, concomitant with the reduction of p62 and ataxin-3 accumulation in cerebellar Purkinje cells, which might partially contribute to the rescue mechanism. In summary, our results reveal that FIR confers therapeutic effects in an SCA3 transgenic animal model and therefore has considerable potential for future clinical use.

Keywords Far-infrared radiation · Spinocerebellar ataxia type 3 · YAC transgenic mice · Behavior · Purkinje cells · Autophagy

Shin-Wu Liu and Jui-Chih Chang are co first-authors

Electronic supplementary material The online version of this article (https://doi.org/10.1007/s12311-018-0936-3) contains supplementary material, which is available to authorized users.

✉ Shou-Jen Kuo
d000103@cch.org.tw

✉ Chin-San Liu
liu48111@gmail.com

[1] Vascular and Genomic Center, Changhua Christian Hospital, 135 Nanhsiao Street, Changhua 50094, Taiwan

[2] Department of Chinese Medicine, China Medical University Hospital, Taichung 40447, Taiwan

[3] School of Chinese Medicine, Graduate Institute of Chinese Medicine, Graduate Institute of Integrated Medicine, College of Chinese Medicine, Research Center for Chinese Medicine and Acupuncture, China Medical University, Taichung 40447, Taiwan

[4] Departments of Medical Research, Obstetrics and Gynecology, Dermatology, and Urology, China Medical University Hospital, Taichung 40447, Taiwan

[5] Department of Life Science, Tunghai University, Taichung 40704, Taiwan

[6] Department of Surgery, Changhua Christian Hospital, 135 Nanhsiao Street, Changhua 50094, Taiwan

[7] Department of Neurology, Changhua Christian Hospital, Changhua 50094, Taiwan

Introduction

Spinocerebellar ataxia (SCA) is a type of neurodegenerative disease caused by genetic mutations resulting in impairment of the nervous system, particularly the spinal cord and cerebellum [1, 2]. Currently, 40 SCA subtypes have been characterized, which have been termed SCA1–40 [1]. SCA3, also called Machado–Joseph disease (MJD), displays a high prevalence in Asia [1, 3]. The onset of these neurodegenerative syndromes begins between the ages of 20 and 50 years and includes progressive gait imbalance and loss of muscle control and coordination [4]. Pathological features of SCA3 include the progressive degeneration of the spinal cord, brainstem, and cerebellum and severe loss of Purkinje cells [2, 5]. The specific cause of SCA3 is an abnormal expansion of CAG repeats in the ataxin-3 gene (ATXN3), which causes an extended polyglutamine (polyQ) sequence in the translated ataxin-3 protein [6]. The ataxin-3 protein controls deubiquitinase activity and is reported to have roles in the chaperone system, ubiquitin–proteosome system, and autophagy pathway. Consequently, ATXN3 mutation impairs the clearance of misfolded proteins [7, 8]. The polyQ mutation also manifests in other neurodegenerative diseases such as Huntington's disease (HD), dentatorubral pallidoluysian atrophy (DRPLA), and X-linked spinal and bulbar muscular atrophy (SMAX1/SBMA) [6, 8, 9].

Infrared therapy has been used for the treatment of various types of diseases in recent years [10–12]. Infrared radiation (IR) is an energy type that covers the wavelength range from 750 to 100 μm [10]. The near infrared (NIR) wavelength spans the range 600–1000 nM, whereas far infrared (FIR) covers the range 3–100 μM. The biophysical mechanism of FIR involves the transfer of its energy to biological tissues and resonation with the tissue molecules, which in turn produces heat and exerts beneficial stimulation of the microenvironment [10, 13]. Studies have shown beneficial effects of FIR treatment in patients and several animal disease models, which include increasing blood flow [14–16], improving peripheral circulation [13], improving endothelial health and functions [17, 18], reducing blood sugar and insulin levels [14], and promoting skin wound healing [19, 20]. FIR has shown therapeutic effects on multiple animal and cell models and has been applied to multiple types of diseases including cardiovascular disease, diabetes, and chronic kidney diseases [11, 15, 21].

In neuromuscular disorders, it has been reported to aid in repairing injured sciatic nerves in a rat model [22] and to reduce lower back pain and improve physical mobility in human patients [23]. NIR has been revealed to confer neuroprotective effects in neuronal diseases [24] and to provide therapeutic benefits in cell and animal models and in human patients with neurodegenerative diseases, mainly Alzheimer's disease and Parkinson's disease [12]. However, the effects of FIR on neurodegenerative disease remain unclear. Our group further evaluated the effect of FIR on SCA3 using an SCA3 cellular model and revealed that FIR prevented its accumulation by promoting autophagy [25], a bulk cellular machinery for degradation and recycling of cellular components in response to environmental stress [26]. However, therapeutic effects of FIR still need to be further confirmed in SCA3 animal models. Autophagy was previously reported to be essential for maintaining protein homeostasis and quality control in neuronal tissues. Autophagy deficiency [27, 28] in mice has been revealed to cause neuronal cell death (e.g., Purkinje cells) and accumulation of aggregated proteins that lead to neurodegeneration. Thus, the purpose of this study was to investigate the potential beneficial effects of FIR on motor ability in an SCA3 transgenic mouse model, the pathology of Purkinje cells in the cerebellum, and the role of autophagy in Purkinje cells.

Materials and Methods

Animal Model MJD15.4 and MJD84.2 transgenic mice were purchased from Jackson Laboratory (Bar Harbor, ME, USA). The genome of the transgenic mouse strains harbors a yeast artificial chromosome (YAC) transgene expressing ATXN3 with either a wild-type polyglutamine tract with 15 CAG repeats (15Q) or a pathological polyglutamine tract with expanded 84 CAG (84Q) repeats [29]. All mice were of C57BL/6J background, and the generation of transgenic mice was achieved as previously described [30]. The identities of the SCA3 transgenic mice were confirmed by PCR from the mouse tail DNA [30]. Mice were maintained under a 12-h light/dark cycle. All animal treatment protocols were approved by the Institutional Animal Care and Use Committee (IACUC) of Changhua Christian Hospital. Mice were randomly divided into three groups ($n = 5$): a normal control group of 15Q mice, SCA3 control group of 84Q mice, and FIR treatment group of 84Q mice.

FIR Exposure The mice were exposed to radiation from a WS TY301 FIR emitter (Far IR Medical Technology, Taipei, Taiwan). The electromagnetic wavelength of the energy emitted from the apparatus is at the range of 3–25 μm with a peak value at 5–7 μm. The radiator was set at a height of 30 cm above the animal cage and was operated with a power density of 50 mW/cm^2 and exposure time of 30 min three times per day (morning, noon, evening). Mice underwent the FIR treatment starting at 4 weeks of age for 7 months.

Motor Behavior Assessment

Rotarod Test Mice were placed on a rotarod at a constant speed of 5 rpm at the beginning. The speed of the rod then

accelerated linearly from 5 to 40 rpm within 300 s according to the procedures described in a previous study [31]. Latency to fall was defined as the time (seconds) the mouse persisted on the rod. The maximal time for each mouse was 5 min, after which the mouse was removed from the rod and allowed to rest for at least 15 min before the next trial to prevent exhaustion. Each mouse underwent four rotarod trials, and the latency to fall was recorded and analyzed statistically. The test was performed once per month for 7 months consecutively.

Balance Beam Test The balance beam test was used to evaluate the motor coordination and balance of the mice [32]. A 60-cm-long plexiglass beam with a diameter of 2 cm was installed approximately 50 cm above the ground between two poles. Mice were placed at the end of the beam and allowed to travel through the beam to the other end (Luong). The travel time from one end to the other for each mouse was recorded. Each mouse was subjected to four trials of traveling, and the recorded travel time was statistically analyzed.

Computer-assisted Method for Gait Analysis Mice were subjected to gait assessment with the CatWalk automated gait analysis system (Noldus Information Technology, Wageningen, Netherlands). The apparatus contains a long glass plate as a runway for animals. When animals traverse from one side of the glass plate to the other, their footsteps are illuminated by fluorescent light emitted from below. The illuminated footsteps are recorded by a high-speed camera installed underneath the glass plate. Mice were subjected to gait assessment with the CatWalk automated gait analysis system (Noldus Information Technology, Wageningen, The Netherlands). The apparatus comprises a glass plate as the walkway floor for the animals to voluntarily traverse. Each mouse performed 3–6 trials, and the statistics of multiple parameters, such as the maximal contact area of the paws (area of the foot touching the plate during the time of maximum contact), stand (duration of the contact of a paw with the glass plate), stride length (distance between two steps of the same paw), base of support (the distance between contralateral paws during initial and terminal stance), swing speed (the stride length divided by swing duration), and print intensities of footsteps, were recorded and analyzed using the software CatWalk XT 9.0. The CatWalk gait analysis was performed when mice were 11.5 months of age (5 months after the last rotarod test).

Preparation of Histological Tissue Sections Mouse cerebellar tissues were harvested and sliced to thin pieces with a thickness of 3 mm and fixed with 4% paraformaldehyde for 48 h, followed by dehydration. Alcohol and fat were removed by soaking the tissue in xylene. The tissue was infiltrated with melted paraffin in a mold. The embedded tissue was removed from the mold after the paraffin hardened. The tissue was sectioned to a thickness of 3 μm using a microtome and transferred to a slide.

Hematoxylin and Eosin Staining The Purkinje cells located between the molecular layer and the granular layer were stained with hematoxylin and eosin (H&E). The sections were deparaffinized and rehydrated sequentially in xylene and 100, 95, 80, and 75% alcohol and water, followed by staining with H&E. Afterward, the sections were sequentially soaked in 80, 95, and 100% alcohol and xylene for dehydration and then sealed.

Immunohistochemical Staining The sections were deparaffinized and rehydrated sequentially in xylene and 100, 95, 80, and 70% alcohol and water, followed by antigen retrieval in an antigen retriever apparatus with heat and pressure. The sections were washed with 1X TBST (10 mM Tris-HCl, 150 mM NaCl, 0.05% [*v*/*v*] tween-20, pH 8.0) and blocked with 3% hydrogen peroxide at room temperature for 10 min. Sections were then incubated in Ultra V Block blocking solution (Thermo Fisher Scientific Inc., MA, USA) and washed with TBST. For staining Purkinje cells, sections were then incubated with anticalbindin D-28L antibody (1:100, Abcam, Cambridge, UK) for 30 min and washed with TBST. After this step, the sections were processed with the UltraVision™ Quanto Detection System HRP DAB kit (Thermo Fisher Scientific Inc., MA, USA) according to the manufacturer's instructions. After incubation with the substrate solution for visualization, sections were washed with tap water. The sections were counterstained with hematoxylin for 1–5 min and washed with tap water for 10 min and then dehydrated in 80, 95, and 100% alcohol and xylene and sealed.

Immunofluorescence Staining First, the sections were incubated in a 60 °C oven for 15 min. The sections were then deparaffinized and rehydrated sequentially in 100% xylene, 1:1 xylene:ethanol, and 100, 95, 70, and 50% alcohol and water. After rehydration, an antigen-retrieval process was performed by boiling the sections in Tris-EDTA buffer (10 mM Tris, 1 mM EDTA, 0.05% Tween-20, pH 9.0) for 30 min, cooled to room temperature, and washed. The sections were then incubated with 0.1% Sudan Black in 70% ethanol for 3 min, followed by incubation with PBS with 1% BSA for 1 h. The sections were washed once with PBS, followed by incubation with primary antibody diluted in PBS with 1% BSA for 2 h. The sections were washed with PBS four times and incubated with secondary antibody conjugated with fluorophores (diluted in PBS with 1% BSA) for 1 h, washed with PBS four times, and mounted with mounting solution containing DAPI (DAPI Fluoromount-G® SouthernBiotech, Birmingham, AL). The sections were then covered with coverslips and sealed using nail polish and subjected to confocal microscopy. The antibodies and dilution factors used are

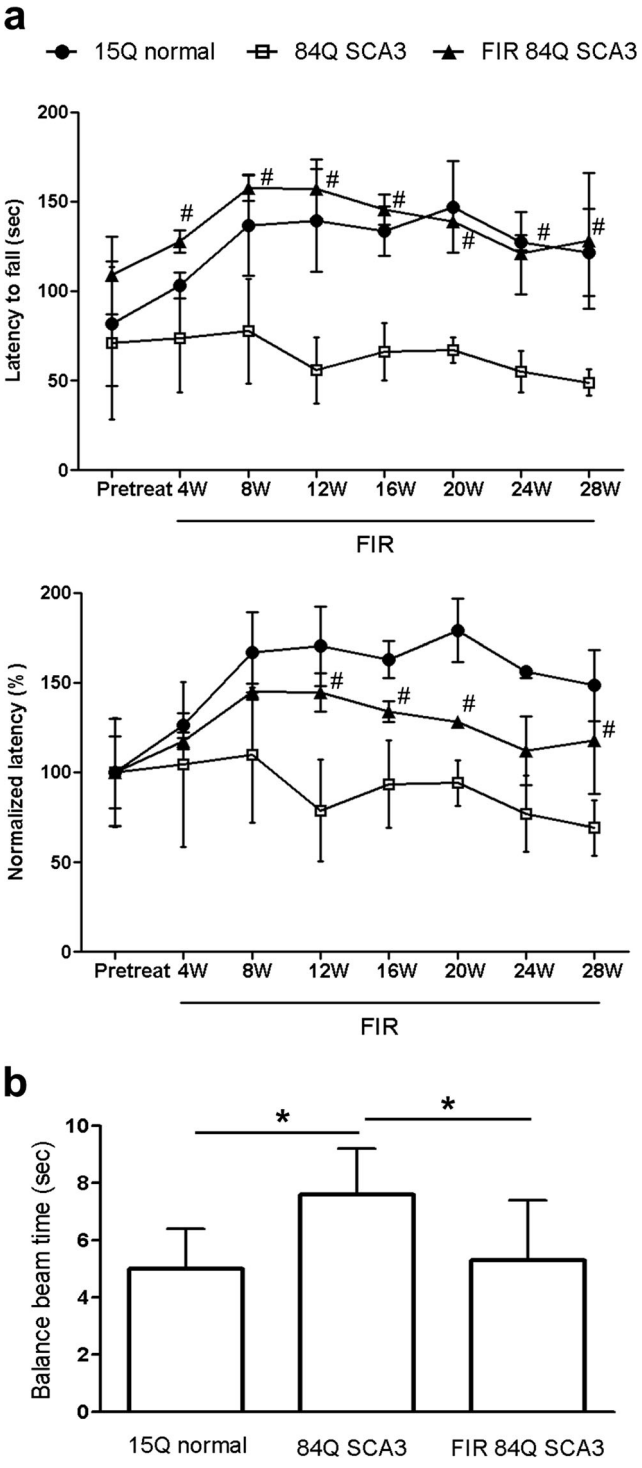

◀ **Fig. 1** Far-infrared radiation (FIR) prevented impairments of motor coordination, balance, and gait in an SCA3 mice model. **a** Representative study plan for mouse motor performance tests. Rotarod test demonstrated prevention of impaired motor coordination of 84Q SCA3 mice. Mice were divided into three groups: 15Q normal, 84Q SCA3, and FIR 84Q SCA3. FIR treatment was carried out daily in groups of FIR 15Q normal and FIR 84Q SCA3 mice at the age of 4 weeks until 36 weeks. An accelerated rotarod test was performed monthly in all three groups of mice, starting at the first FIR treatment. Above panel—the latency to fall (seconds that mice persisted on the rotarod) is plotted against the time frame. Below panel—the latency to fall at the first FIR treatment (pretreat) is normalized to 100%. **b** Balance beam walking test demonstrated prevention of imbalance in 84Q SCA3 mice. The test was conducted in all groups at the age of 12 months. The time (seconds) required by each mouse to travel through the balance beam was recorded and analyzed. Statistical significance was determined by Student's *t* test. # $p < 0.05$ denotes statistical significance within SCA3 84Q groups with and without FIR. * $p < 0.05$ is considered statistically significant and is indicated by an asterisk

presented as follows: mouse anticalbindin antibody (1:50, Abcam, Cambridge, UK), anti-ataxin-3 antibody (1:50, Chemicon, Temecula, CA), rabbit anti-p62/SQSTM1 antibody (1:500, Sigma-Aldrich, St. Louis, MO), rabbit anti-Beclin-1 (1:50, Novus Biological, Littleton, CO antibody), rabbit anti-LC3B (1:200 Novus Biological, Littleton, CO), goat anti-rabbit secondary antibody conjugated with DyLight™ 488 (1:500, KPL, Gaitherburg, MD), and goat antimouse secondary antibody conjugated with Alexa Fluor™ 647 (1:500, Jackson ImmunoResearch Laboratories, West Grove, PA). After the staining process, the stained slices were imaged by an Olympus FluoView FV 1200 Confocal Microscope (Olympus, Tokyo, Japan), and the integration of line scans in the same cell image through the *z*-axis yielded a longitudinal view of the synaptic sites, which were analyzed using CellSens Dimension Desktop version 1.3 (Olympus Corporation) software.

Statistical Analysis The two-tailed Student's *t* test and the Mann–Whitney *U* test were used to determine the significance of differences between groups as indicated in the figure legends. A difference with $p < 0.05$ was considered to be statistically significant and is indicated by an asterisk.

Results

FIR Maintained the Motor Ability and Balance of SCA3 Mice

The rotarod test, beam walking test, and CatWalk gait were conducted to evaluate the motor ability and gait performance of the control and SCA3 mice with or without FIR treatment for 28 weeks. The mice were subjected to the rotarod test at 4 weeks of age for evaluation of their motor coordination performance and endurance. As shown in Fig. 1a, the nontreated 84Q SCA3 group displayed a shorter latency to fall time compared with the 15Q normal and FIR 84Q SCA3 groups throughout the experimental process. After 28 weeks, the average latency to fall time of the 84Q SCA3 mice was 48.9 ± 7.5 s. The 15Q normal mice had an average time of 121.6 ± 24.2 s, which was similar to that of the FIR 84Q SCA3 mice (128.1 ± 38.1 s). After normalization to the pretreatment point, the percentage of relative latency to fall of the FIR 84Q SCA3 mice was still higher than that of the 84Q SCA3 mice (117.8 ± 29.8% vs. 69.1 ± 15.3%), although not

as high as that of the 15Q normal group (148.5% ± 19.9%) (below panel, Fig. 1a). This trend remained consistent throughout the 7-month period.

For the balance beam test, as shown in Fig. 1b, the 84Q SCA3 mice displayed 35% more traveling time compared with the 15Q normal mice, indicating a loss of coordination and balance ability (15Q normal vs. 84Q SCA3 = 5.0 ± 1.4 vs. 7.6 ± 1.6). The FIR 84Q SCA3 group displayed reduced traveling time that was comparable to that of the 15Q normal group (FIR 84Q SCA3 vs. 84Q SCA3: 5.3 ± 2.1 vs. 7.6 ± 1.6). These results reflected that 7 months of FIR treatment successfully rescued the balance ability impaired by SCA3.

Figure 2 presents the statistics of the six parameters analyzed: maximal contact area of the paws (Fig. 2a), stand (Fig. 2b), stride length (Fig. 2c), base of support (Fig. 2d), swing speed (Fig. 2e), and print intensities of footsteps (Fig. 2f). For these six parameters, the test values of the 84Q SCA3 mice differed significantly from those of the 15Q normal mice for at least one of the two leg sets, indicating a change in gait performance due to SCA3. In the group with FIR treatment, the gait performance significantly improved relative to that of the SCA3 group without treatment in terms of contact area (Fig. 2a), stride length (Fig. 2c), and base support (Fig. 2d) in forepaws, hindpaws, or both. These results consistently showed FIR treatment to confer partial protective effects on the SCA3 mice.

FIR Restored the Loss of Purkinje Cells in the Cerebellum After the motor ability tests, the 12-month-old mice were sacrificed. Their cerebella were harvested and used for histocytological analysis, which consisted of visualization of the individual Purkinje cell layers (PCL), granular layers and molecular layers, and other structures of the cells. After H&E staining and immunohistochemical for calbindin, the sections were photographed and the number of Purkinje cells (indicated with arrows in Fig. 3a) along the PCL of the posterior lobules of the

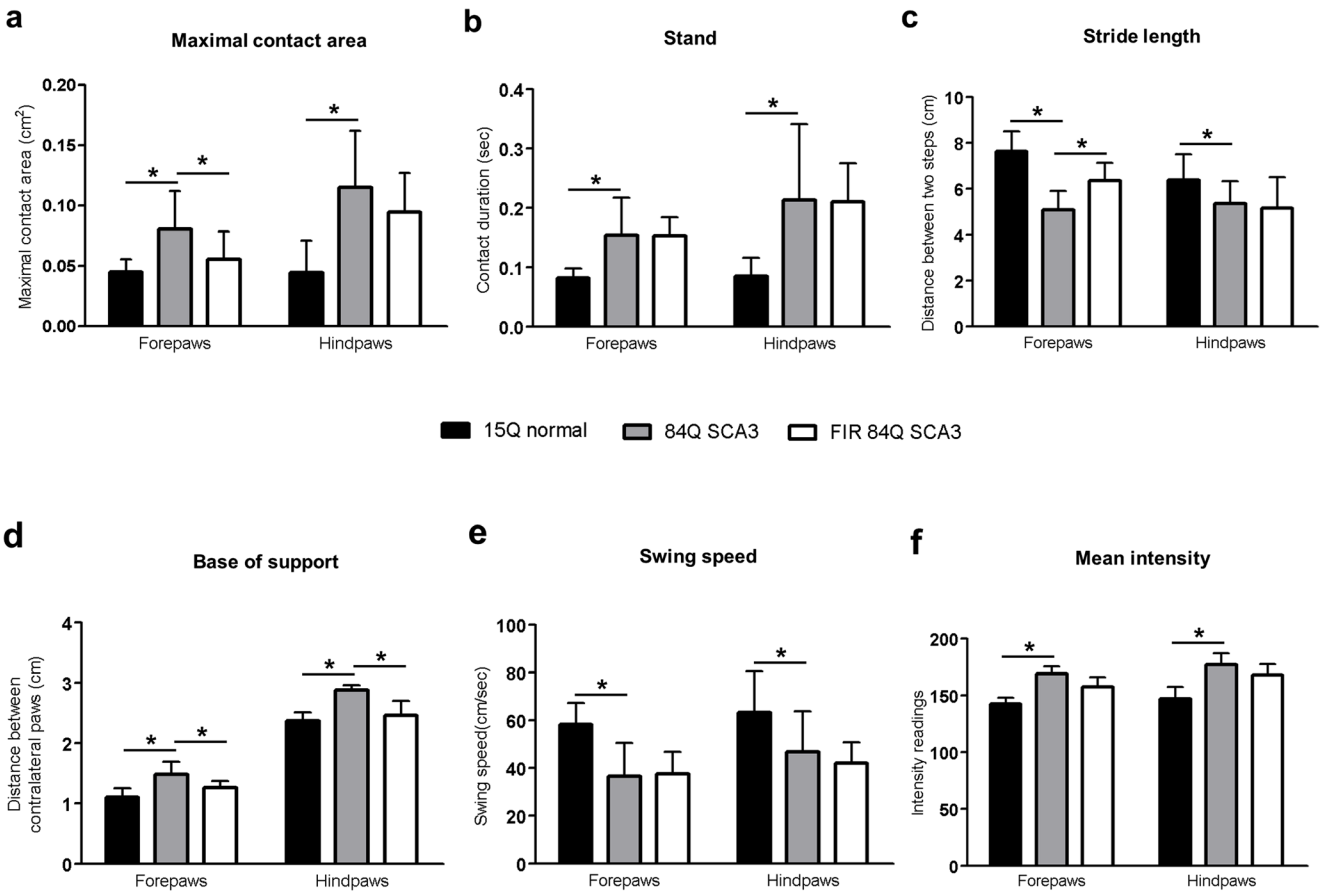

Fig. 2 Far-infrared radiation partially prevented gait changes in SCA3 mice. Gait analysis of the mice was conducted at the age of 11.5 months using a CatWalk automatic gait analysis system. Mice were placed on a glass plate on the apparatus and allowed to traverse from one end to the other. Three to six trials were performed for each mouse. Their footsteps were recorded and analyzed by software in the computer linked to the apparatus. Six parameters were analyzed: **a** maximal contact area of the paws (area of the foot touching the plate during the time of maximum contact), **b** stand (duration of the contact of a paw with the glass plate), **c** stride length (distance between two steps of the same paw), **d** base of support (distance between contralateral paws during initial and terminal stance), **e** swing speed (stride length divided by swing duration), and **f** print intensities of footsteps. Statistical significance was determined by Student's *t* test. * $p < 0.05$ is considered a statistically significant difference and is indicated by an asterisk

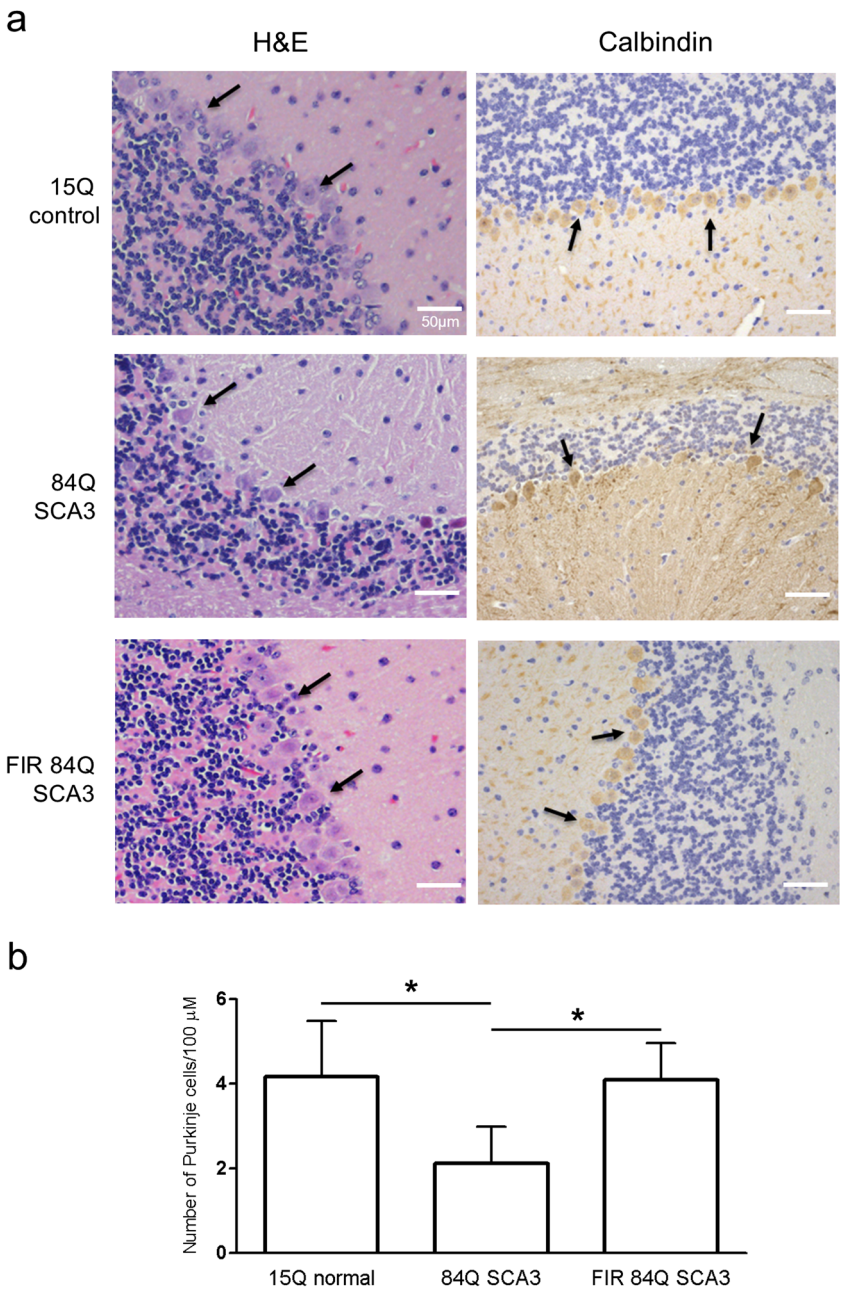

Fig. 3 Far-infrared radiation (FIR) prevented the death of Purkinje cells in the cerebellum of 84Q SCA3 mice. Cerebellar sections from three groups of mice were deparaffinized and subjected to hematoxylin and eosin (H&E) staining and immunohistochemical (IHC) staining using anticalbindin antibodies. These groups were 15Q normal, 84Q SCA3, and FIR 84Q SCA3. **a** H&E and IHC staining of the cerebella of mice from the groups of 15Q normal, 84Q SCA3, and FIR 84Q SCA3. The arrows indicate Purkinje cells located at the Purkinje cell layer between the molecular layer and granular layer. **b** Quantitation of average Purkinje cell numbers in the posterior lobules of the cerebellum. The number of Purkinje cells located along the proximal–distal axis length of approximately 25 mm on the sections was calculated. Cerebellar sections from two mice from each group were chosen, and 9 to 12 microscopic fields of posterior lobules were examined accordingly in each section. The average cell number per 100 μm is presented in the bar graph. Statistical significance was determined by the Mann–Whitney test. * $p < 0.05$ was considered a statistically significant difference and is indicated by an asterisk

cerebellum (a proximal–distal axis length of approximate 25 mm) was counted. The average number of the Purkinje cells per 100 μm in the PCL was quantified (Fig. 3b). The 84Q SCA3 mice without FIR treatment had significantly a lower number of Purkinje cells compared with the 15Q normal mice (15Q normal vs. 84Q SCA3 = 4.167 ± 1.364 vs. 3.118 ± 0.871), which was restored to a normal level after FIR treatment (FIR 84Q SCA3 vs. 84Q SCA3 = 4.100 ± 0.865 vs. 3.118 ± 0.871).

FIR Promoted Autophagy and Alleviated the Accumulation of Mutant Ataxin-3 The levels of ataxin-3 (both wild-type and mutant forms) and autophagy were evaluated through immunofluorescence staining. The autophagy marker proteins used included p62, Beclin-1, and LC3II in the Purkinje cells of mouse cerebellar. The Purkinje cells (as indicated by arrows in Fig. 4a) in the 84Q SCA3 group expressed obvious ataxin-3 protein (red color) and p62 protein (green color) levels compared with those in the 15Q normal and FIR 84Q SCA3 groups (Fig. 4a). The quantification of p62 and ataxin-3 showed a significant increase in the proteins in the Purkinje cells of the 84Q SCA3 mice by approximately 80 and 40%, respectively (Fig. 4b). With FIR treatment, the levels of p62 and ataxin-3 were reduced to a normal level (Fig. 4b). In the 84Q SCA3 mice, ataxin-3 had an extensive distribution and formed clear foci throughout, colocalizing with p62, as

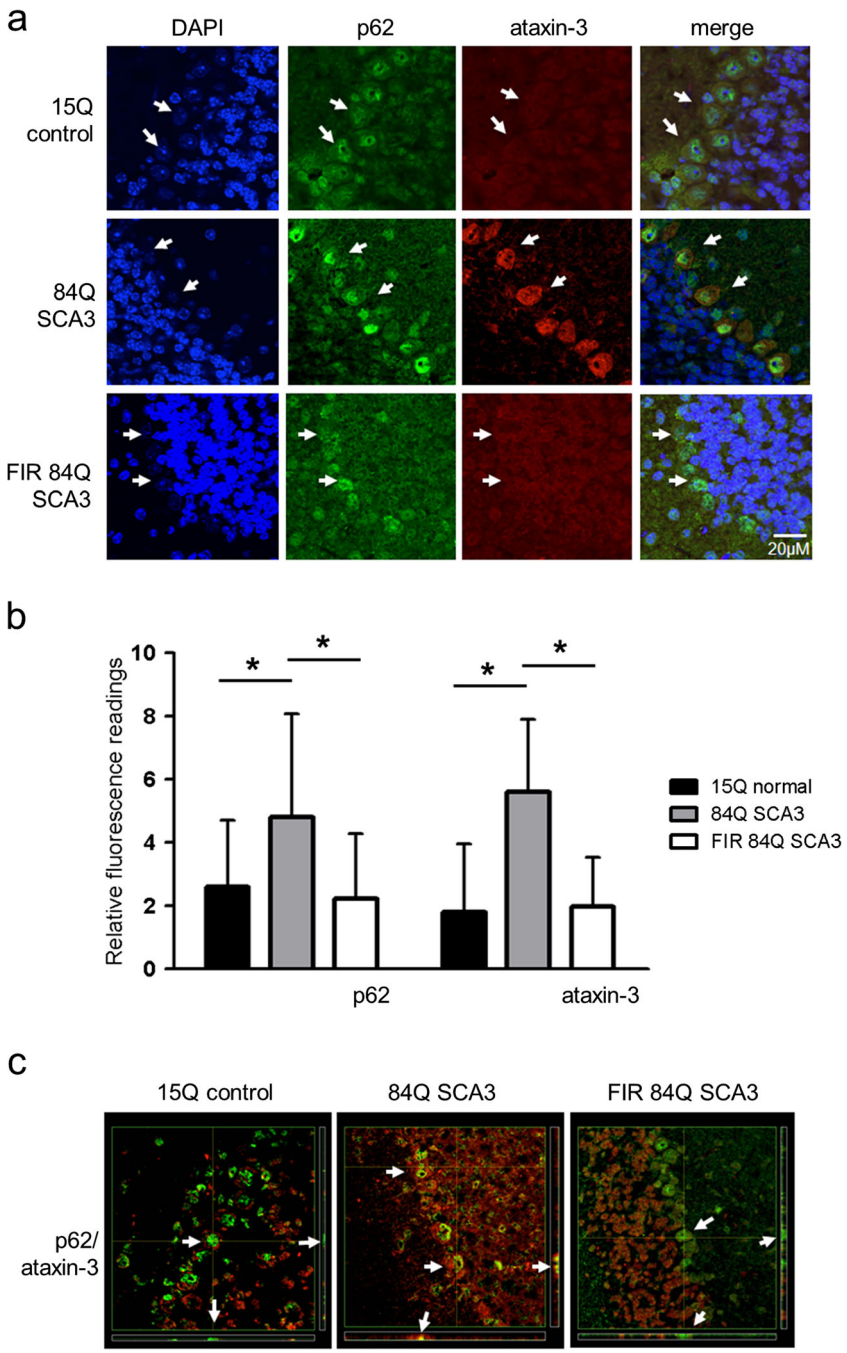

Fig. 4 Far-infrared radiation (FIR) prevented the accumulation of p62 and ataxin-3 in 84Q SCA3 mice. **a** Deparaffinized and antigen-retrieved cerebellar sections from three groups of mice were subjected to immunofluorescence staining for the detection of p62 and ataxin-3 levels. These groups were 15Q normal, 84Q SCA3, and FIR 84Q SCA3. The expression of p62 and ataxin-3 in Purkinje cells was detected using antibodies conjugated with fluorophores with distinct colors followed by examination with confocal microscopy. p62, green; ataxin3, red. The arrows indicate Purkinje cells. **b** Fluorescence intensities of p62 and ataxin-3 were determined using ImageJ software. The fluorescence intensities from 35 to 70 Purkinje cells in each slice individually chosen from two mice of each group were quantitated. The quantitation is presented in the bar graphs. Statistical significance was determined by the Mann–Whitney test. * $p < 0.05$ was considered a statistically significant difference and is indicated by an asterisk. **c** Colocalization status of p62 and ataxin-3 presented by a projection of Z-series through FlowView software. The colocalization is indicated with arrows as a yellow color of merged green (p62) and red (ataxin-3) fluorescence

indicated by the arrows (Fig. 4c, yellow color, combination of both colors representing colocalization). This reflected an obstacle to the autophagic degradation of aggregative ataxin-3 that causes ataxin-3/p62 complex accumulation in SCA3 mice. By contrast, only a small amount of aggregative ataxin-3 protein colocalized with the p62 protein in the 15Q control and FIR treatment groups. Furthermore, the number of axaxin-3/p62 complexes was lower than that in the 84Q SCA3 group (Fig. 4c). The autophagy status was further confirmed by the other autophagy markers of Beclin-1 (Fig. 5a) and LC3II (Fig. 5b). Additionally, punctate pattern of LC3II was identified by the pixels of cellular LC3II expression levels above the local of remaining pixels. Punctate pattern expression in LC3II immunofluorescence staining was calculated by normalizing the total intensity of LC3BII in cells, as shown by dashed circles in the merged panel of Fig. 5b. There was no dramatic change in either protein in the 84Q SCA3 mice compared with the 15Q normal group, but FIR treatment

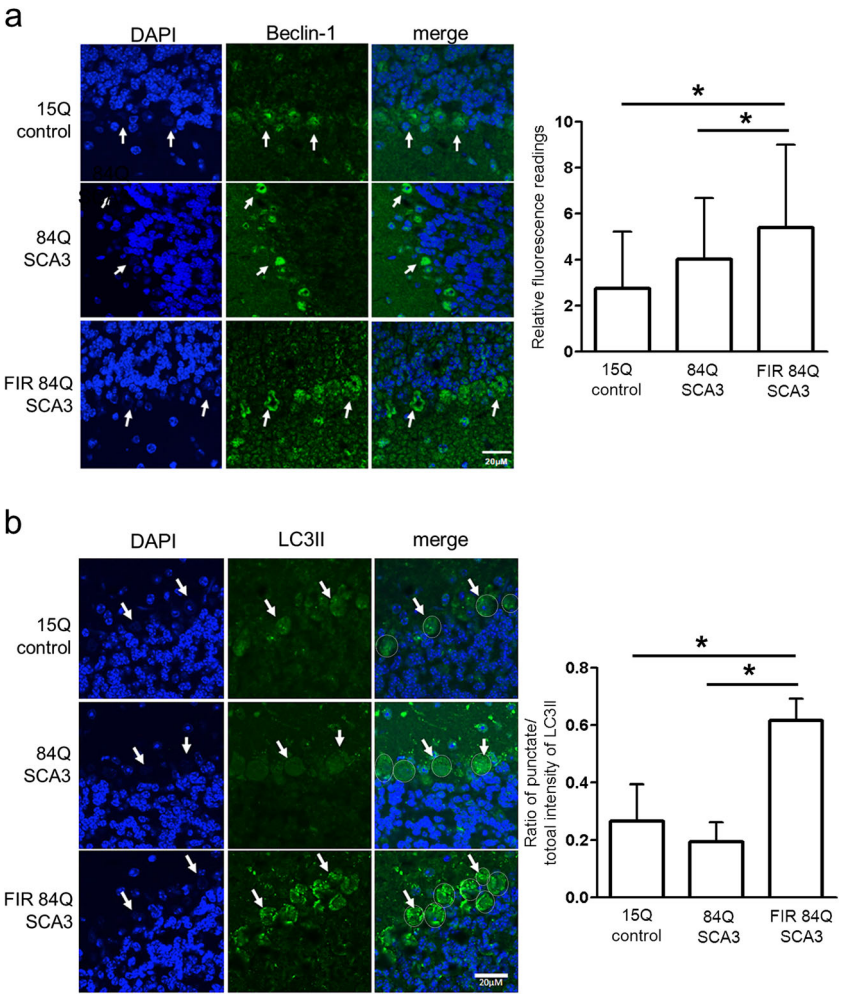

Fig. 5 Far-infrared radiation promoted autophagy. **a** Expression of Beclin-1 and **b** LC3II in mouse cerebella was examined by immunofluorescence staining and quantified by ImageJ software (right panel). Arrows indicate Purkinje cells, of which 30–35 in each slice individually chosen from two mice from each group were quantitated for fluorescence intensities. For quantification of autophagy activation, punctate pattern of LC3II was identified by the pixels of cellular LC3II expression level above the local of the remaining pixels. Punctate pattern expression in LC3II immunofluorescence staining was calculated by normalizing the total intensity of LC3BII in cells, which is represented as the dashed circle in the merged panel. Statistical significance was determined by the Mann–Whitney test. * $p < 0.05$ represents statistically significant differences in values

significantly increased Beclin-1 expression (Fig. 5a) and the punctate pattern levels in LC3II staining (Fig. 5b).

Discussion

This study showed that 84Q SCA3 mice displayed greater motor deficits and neuronal cell death compared with the control mice and that FIR treatment effectively prevented the aforementioned pathological outcomes. FIR treatment also promoted autophagy, as reflected by the induction of LC3II and Beclin-1 concomitant with the decrease of p62 and ataxin-3 accumulation, which might partially contribute to the rescue mechanism. This study validated again that FIR therapy is a convenient and noninvasive therapeutic modality for SCA3. These results are consistent with the autophagy mechanism seen in our previous research in which an SK-N-SH neuroblastoma cell SCA3 in vivo rat model system expressed toxic ataxin-3 protein with a 78 polyglutamine segment [25].

NIR has been found to effectively improve motor and physical functions in animal models and patients with neurodegenerative diseases. For example, NIR improved the locomotive behaviors of Parkinson's mouse models and reduced the clinical signs and symptoms in a monkey model and Parkinson's patients [12]. In this study, we found a consistent result by using the diversifiable assessment of motor behavior to characterize the motor impairments in a mouse population. We showed that all measures of locomotor activity, balance/coordination, and gait performance were affected by cerebellar lesions. Moreover, FIR treatment had a generalized effect that included improvement of coordination on the rotating rod, improvement of stationary stability during beam walking, and modification of the maximal contact area of paws, base of support, and stride length to normal control levels. Compared with another treatment for SCA3 mice, namely, neuronal nicotinic receptor agonists, there was a more generalized and consistent effect in the improvement of motor behavior [33]. FIR has been reported to improve physical function in neuromuscular disorders such as sciatic nerve injury, lower back pain, and stroke [22, 23, 34], but there is little literature focusing on the aspect of motor behavior. Our results reveal its therapeutic effect in a mouse model of a

neurodegenerative disease different from the aforementioned neuromuscular disorders.

Reports have revealed that autophagy is involved in maintaining normal neuronal functions. Impaired autophagy due to genetic mutation in autophagic proteins or damaged autophagosomes has been described in human SCA3 patients [35, 36] and other neurodegenerative diseases such as Huntington's disease, SBMA, and SCA7 [37]. In animal models of SCA3 and Parkinson's disease, induction of autophagy has been shown to reduce the toxic mutant proteins ataxin-3 and huntingtin with polyglutamine expansions [38, 39]. A recent biochemical study found that ataxin-3 interacts with an autophagy inducer, Beclin-1, by protecting it from degradation. The mutant form ataxin-3 with an expansion of polyglutamine failed to confer these protective effects, which causes impairment of autophagy. Upregulated autophagy improved motor function of mice, reduced protein aggregates, and reversed cellular pathology [39, 40]. FIR has been implicated in changing the autophagy status of cells. In our previous SCA3 cellular model, the SCA3 cells expressing the gene with a polyglutamine expansion displayed autophagy defects that were corrected by FIR treatment [25]. In the present study conducted on SCA3 mice, the levels of the autophagy inducer Beclin-1 and autophagosome marker LC3II were significantly lower compared with those observed in the control mice, and the level of the autophagy cargo receptor p62 was significantly higher, suggesting aberrant clearance of the accumulated mutant ataxin-3 protein. The p62 protein is a carrier that transfers target proteins to the autophagosome for degradation in autophagy. It has been reported to accumulate in an autophagy-deficient mouse model [41] and to colocalize with the accumulated ataxin-3 in SCA3 patients [40] and SCA3 mouse models [40, 42]. The accumulation of p62 in Purkinje cells was also reported in another SCA3 mouse model [40]. The loss of Purkinje cells is a common feature of many types of SCA in patients [2, 43], as well as the SCA3 mouse model [29]. Upon treatment with FIR, the survival of Purkinje cells was increased, as well as the levels of Beclin-1 and LC3II. Conversely, the levels of p62 and ataxin-3 were reduced in FIR-treated SCA3 mice compared with untreated SCA3 mice. Our data imply that FIR promoted autophagy, which might have in turn prevented the neuronal pathology of SCA3.

Recently, FIR treatment was shown to activate autophagy through induction of PI3K-mediated nuclear translocation of a transcription factor, promyelocytic leukemia zinc finger (PLZF) protein, which promoted the degradation of toxic advanced glycation end products (AGEs) in endothelial cells [18]. The reduction of AGEs was also confirmed in the vascular endothelium of the large intestine of an FIR-treated diabetic mouse model [18]. Moreover, FIR exposure induced autophagy in THP-1 macrophages, which in turn suppressed the NLRP3 inflammasome and induced the ubiquitination of ASC, an adaptor protein of the inflammasome complex, both in cells and in a rat model with second-degree burns. FIR exposure also induced autophagy and inhibited NLRP3 inflammasome activities both in vitro and in a rat model of deep second-degree burns [20].

This pioneering animal study investigated FIR treatment as a potential therapeutic strategy for SCA3 patients. Our results provide evidence that FIR treatment prevents motor deficits in an SCA3 mouse model. FIR was also observed to promote autophagy, which might partially contribute to the rescue mechanism of FIR. The detailed mechanism remains to be investigated further. Previously, Xuan et al. reported that a laser treatment strategy in the NIR range exerted neuroprotective effects by stimulating proliferation of neuronal cells in a mouse traumatic brain injury model [44]. To investigate whether neurogenesis is involved in the neuroprotective effects of FIR on SCA3 mice, future experiments would be needed to test the relevant neuronal proliferation by staining the cerebellar sections with BrdU or proliferation markers. Indeed, in an ongoing study, we have found preliminary evidence that FIR increased the survival rate of SCA3 *Drosophila* by 50%. These results imply that FIR exerted cell protective effects in a *Drosophila* SCA3 disease model (Fig. S1). In addition, the deubiquitinase activity of axin-3 protects Beclin-1 from degradation [45]. Therefore, the functional role of ubiquitin-related enzymes in autophagy regulation should be explored in the future.

Acknowledgments We thank Dr. Chen Chang (Institute of Biomedical Sciences, Academia Sinica) for advice and assistance on preliminary experimental research.

Funding Information This study was supported by the National Science Council (NSC 103-2314-B-371-005-; MOST 103-2320-B-371-001-).

Compliance with Ethical Standards

Conflict of Interest The authors declare that they have no conflict of interest.

References

1. Sun YM, Lu C, Wu ZY. Spinocerebellar ataxia: relationship between phenotype and genotype—a review. Clin Genet. 2016;90:305–14.
2. Taroni F, DiDonato S. Pathways to motor incoordination: the inherited ataxias. Nat Rev Neurosci. 2004;5:641–55.
3. Bird TD. Hereditary ataxia overview. 2016.
4. do Carmo Costa M, Paulson HL. Toward understanding Machado–Joseph disease. Prog Neurobiol. 2012;97:239–57.
5. Koeppen AH. The pathogenesis of spinocerebellar ataxia. Cerebellum. 2005;4:62–73.

6. Seidel K, Siswanto S, Fredrich M, Bouzrou M, Brunt E, Leeuwen F, et al. Polyglutamine aggregation in Huntington's disease and spinocerebellar ataxia type 3: similar mechanisms in aggregate formation. Neuropathol Appl Neurobiol. 2016;42:153–66.
7. Li X, Liu H, Fischhaber PL, Tang T-S. Toward therapeutic targets for SCA3: insight into the role of Machado–Joseph disease protein ataxin-3 in misfolded proteins clearance. Prog Neurobiol. 2015;132:34–58.
8. Fan H-C, Ho L-I, Chi C-S, Chen S-J, Peng G-S, Chan T-M, et al. Polyglutamine (PolyQ) diseases: genetics to treatments. Cell Transplant. 2014;23:441–58.
9. Piccioni F, Pinton P, Simeoni S, Pozzi P, Fascio U, Vismara G, et al. Androgen receptor with elongated polyglutamine tract forms aggregates that alter axonal trafficking and mitochondrial distribution in motor neuronal processes. FASEB J. 2002;16:1418–20.
10. Vatansever F, Hamblin MR. Far infrared radiation (FIR): its biological effects and medical applications. Photonics Lasers Med. 2012;1:255–66.
11. Shui S, Wang X, Chiang JY, Zheng L. Far-infrared therapy for cardiovascular, autoimmune, and other chronic health problems: a systematic review. Exp Biol Med. 2015;240:1257–65.
12. Johnstone DM, Moro C, Stone J, Benabid A-L, Mitrofanis J. Turning on lights to stop neurodegeneration: the potential of near infrared light therapy in Alzheimer's and Parkinson's disease. Front Neurosci. 2016;9:500.
13. Yu SY, Chiu JH, Yang SD, Hsu YC, Lui WY, Wu CW. Biological effect of far-infrared therapy on increasing skin microcirculation in rats. Photodermatol Photoimmunol Photomed. 2006;22:78–86.
14. Ryotokuji K, Ishimaru K, Kihara K, Namiki Y, Hozumi N. Preliminary results of pinpoint plantar long-wavelength infrared light irradiation on blood glucose, insulin and stress hormones in patients with type 2 diabetes mellitus. Laser Ther. 2013;22:209–14.
15. Wan Q, Yang S, Li L, Chu F. Effects of far infrared therapy on arteriovenous fistulas in hemodialysis patients: a meta-analysis. Ren Fail. 2017;39:613–22.
16. Lin C-C, Liu X-M, Peyton K, Wang H, Yang W-C, Lin S-J, et al. Far infrared therapy inhibits vascular endothelial inflammation via the induction of heme oxygenase-1. Arterioscler Thromb Vasc Biol. 2008;28:739–45.
17. Kihara T, Biro S, Imamura M, Yoshifuku S, Takasaki K, Ikeda Y, et al. Repeated sauna treatment improves vascular endothelial and cardiac function in patients with chronic heart failure. J Am Coll Cardiol. 2002;39:754–9.
18. Chen C-H, Chen T-H, Wu M-Y, Chou T-C, Chen J-R, Wei M-J, et al. Far-infrared protects vascular endothelial cells from advanced glycation end products-induced injury via PLZF-mediated autophagy in diabetic mice. Sci Rep. 2017;7.
19. Toyokawa H, Matsui Y, Uhara J, Tsuchiya H, Teshima S, Nakanishi H, et al. Promotive effects of far-infrared ray on full-thickness skin wound healing in rats. Exp Biol Med. 2003;228:724–9.
20. Chiu H-W, Chen C-H, Chang J-N, Chen C-H, Hsu Y-H. Far-infrared promotes burn wound healing by suppressing NLRP3 inflammasome caused by enhanced autophagy. J Mol Med. 2016;94:809–19.
21. Bashar K, Healy D, Browne LD, Kheirelseid EA, Walsh MT, Clarke M, et al. Role of far infra-red therapy in dialysis arteriovenous fistula maturation and survival: systematic review and meta-analysis. PLoS One. 2014;9:e104931.
22. Chen T-Y, Yang Y-C, Sha Y-N, Chou J-R, Liu B-S. Far-infrared therapy promotes nerve repair following end-to-end neurorrhaphy in rat models of sciatic nerve injury. Evid Based Complement Alternat Med. 2015;2015.
23. Ervolino F, Gazze R. Far infrared wavelength treatment for low back pain: evaluation of a non-invasive device. Work. 2016;53:157–62.
24. Yu Z, Liu N, Zhao J, Li Y, McCarthy TJ, Tedford CE, et al. Near infrared radiation rescues mitochondrial dysfunction in cortical neurons after oxygen-glucose deprivation. Metab Brain Dis. 2015;30:491–6.
25. Chang J-C, Wu S-L, Hoel F, Cheng Y-S, Liu K-H, Hsieh M, et al. Far-infrared radiation protects viability in a cell model of spinocerebellar ataxia by preventing polyQ protein accumulation and improving mitochondrial function. Sci Rep. 2016;6.
26. Budini M, Buratti E, Morselli E, Criollo A. Autophagy and its impact on neurodegenerative diseases: new roles for TDP-43 and C9orf72. Front Mol Neurosci. 2017;10.
27. Komatsu M, Waguri S, Chiba T, Murata S, Iwata J-i, Tanida I, et al. Loss of autophagy in the central nervous system causes neurodegeneration in mice. Nature. 2006;441:880–4.
28. Hara T, Nakamura K, Matsui M, Yamamoto A, Nakahara Y, Suzuki-Migishima R, et al. Suppression of basal autophagy in neural cells causes neurodegenerative disease in mice. Nature. 2006;441:885–9.
29. Cemal CK, Carroll CJ, Lawrence L, Lowrie MB, Ruddle P, Al-Mahdawi S, et al. YAC transgenic mice carrying pathological alleles of the MJD1 locus exhibit a mild and slowly progressive cerebellar deficit. Hum Mol Genet. 2002;11:1075–94.
30. Chen X, Tang T-S, Tu H, Nelson O, Pook M, Hammer R, et al. Deranged calcium signaling and neurodegeneration in spinocerebellar ataxia type 3. J Neurosci. 2008;28:12713–24.
31. Shiotsuki H, Yoshimi K, Shimo Y, Funayama M, Takamatsu Y, Ikeda K, et al. A rotarod test for evaluation of motor skill learning. J Neurosci Methods. 2010;189:180–5.
32. Luong TN, Carlisle HJ, Southwell A, Patterson PH. Assessment of motor balance and coordination in mice using the balance beam. J Visual Exp. 2011.
33. Wecker L, Engberg M, Philpot R, Lambert C, Kang C, Antilla J, et al. Neuronal nicotinic receptor agonists improve gait and balance in olivocerebellar ataxia. Neuropharmacology. 2013;73:75–86.
34. Lampl Y, Zivin JA, Fisher M, Lew R, Welin L, Dahlof B, et al. Infrared laser therapy for ischemic stroke: a new treatment strategy. Stroke. 2007;38:1843–9.
35. Onofre I, Mendonça N, Lopes S, Nobre R, De Melo JB, Carreira IM, et al. Fibroblasts of Machado Joseph disease patients reveal autophagy impairment. Sci Rep. 2016;6.
36. Kim M, Sandford E, Gatica D, Qiu Y, Liu X, Zheng Y, et al. Mutation in ATG5 reduces autophagy and leads to ataxia with developmental delay. elife. 2016;5:e12245.
37. Cortes CJ, La Spada AR. Autophagy in polyglutamine disease: imposing order on disorder or contributing to the chaos? Mol Cell Neurosci. 2015;66:53–61.
38. Ravikumar B, Vacher C, Berger Z, Davies JE, Luo S, Oroz LG, et al. Inhibition of mTOR induces autophagy and reduces toxicity of polyglutamine expansions in fly and mouse models of Huntington disease. Nat Genet. 2004;36:585–95.
39. Menzies FM, Huebener J, Renna M, Bonin M, Riess O, Rubinsztein DC. Autophagy induction reduces mutant ataxin-3 levels and toxicity in a mouse model of spinocerebellar ataxia type 3. Brain. 2009;133:93–104.
40. Nascimento-Ferreira I, Santos-Ferreira T, Sousa-Ferreira L, Auregan G, Onofre I, Alves S, et al. Overexpression of the autophagic beclin-1 protein clears mutant ataxin-3 and alleviates Machado–Joseph disease. Brain. 2011;134:1400–15.
41. Komatsu M, Waguri S, Koike M, Sou Y-s, Ueno T, Hara T, et al. Homeostatic levels of p62 control cytoplasmic inclusion body formation in autophagy-deficient mice. Cell. 2007;131:1149–63.
42. Ramani B, Harris GM, Huang R, Seki T, Murphy GG, MdC C, et al. A knockin mouse model of spinocerebellar ataxia type 3 exhibits prominent aggregate pathology and aberrant splicing of the disease gene transcript. Hum Mol Genet. 2014;24:1211–24.

43. Schilling K, Oberdick J, Rossi F, Baader SL. Besides Purkinje cells and granule neurons: an appraisal of the cell biology of the interneurons of the cerebellar cortex. Histochem Cell Biol. 2008;130: 601–15.
44. Xuan W, Vatansever F, Huang L, Hamblin MR. Transcranial low-level laser therapy enhances learning, memory, and neuroprogenitor cells after traumatic brain injury in mice. J Biomed Opt. 2014;19: 108003.
45. Ashkenazi A, Bento CF, Ricketts T, Vicinanza M, Siddiqi F, Pavel M, et al. Polyglutamine tracts regulate beclin 1-dependent autophagy. Nature. 2017;545:108–11.